


Research Article

The Effects of Activation Energy and Thermophoretic Diffusion of Nanoparticles on Steady Micropolar Fluid along with Brownian Motion

Zulqurnain Sabir,¹ Assad Ayub,¹ Juan L. G. Guirao ,² Saira Bhatti,³ and Syed Zahir Hussain Shah¹

¹Department of Mathematics & Statistics, Hazara University, Manshera, Pakistan

²Department of Applied Mathematics and Statistics, Technical University of Cartagena, Hospital de Marina 30203-Cartagena, Cartagena, Spain

³Department of Mathematics, COMSATS University Islamabad, Abbottabad Campus, Abbottabad, Pakistan

Correspondence should be addressed to Juan L. G. Guirao; juan.garcia@upct.es

Received 18 March 2020; Revised 16 June 2020; Accepted 22 June 2020; Published 9 July 2020

Academic Editor: Candido Fabrizio Pirri

Copyright © 2020 Zulqurnain Sabir et al. This is an open access article distributed under the Creative Commons Attribution License, which permits unrestricted use, distribution, and reproduction in any medium, provided the original work is properly cited.

The present study is related to the effects of activation energy and thermophoretic diffusion on steady micropolar fluid along with Brownian motion. The activation energy and thermal conductivity of steady micropolar fluid are also discussed. The equation of motion, angular momentum, temperature, concentration, and their boundary conditions are presented for the micropolar fluid. The detail of geometry reveals the effects of several parameters on the parts of the system. The nonlinear partial differential equations are converted into nonlinear ordinary differential equations, and a famous shooting scheme is used to present the numerical solutions. The comparison of the obtained results by the shooting technique and the numerical *bvp4c* technique is presented. The behavior of local skin friction numbers and couple stress number is tabulated for different parameters, and some figures are plotted to present the different parameters. For uplifting the values of AE for parameter λ^A , the concentration profile is increased because of the Arrhenius function, and AE increases with the reduction of this function. The increasing values of the parameter of rotation G show the decrement in velocity because of the rotation of the particle of the fluid, so the linear motion decreases. Thermophoresis is responsible for shifting the molecules within the fluid, and due to this, an increment in boundary layer thickness is found, so by a greater value of Nt , the concentration profile decreases and temperature profile goes down.

1. Introduction

Eringen presented the microfluid theory that describes the mathematical model of the behavior of non-Newtonian fluid, exotic lubricants, polymeric fluids, liquid crystals, ferro liquids, and colloidal fluids [1]. The most important theoretical concept was presented by Eringen using the microfluids, and a famous micropolar fluid (MP) model was introduced [2, 3]. To demonstrate certain microscopic effects, many researchers are taking interest in the micro-rotation and local structure of fluid nanoparticles. Such fluids determined by spin inertia are capable to support the

body and stress moments. The theory related to microfluids is not easy to understand due to nontrivial problems [4]. The subclass of microfluids is the MP fluid that involves microrotational effects and microrotational inertia. The MP is a base of the chemical Navier–Stokes model, and the tiny structure of this fluid makes the nature hard to understand. The MP fluid is very important and has vast applications in many industrial processes. Eringen [1] extended the idea to formulate the theory of thermomicropolar fluid. Later on, many researchers studied the following attributes of the edge layer of these fluids over a semi-infinite plate of high temperature. Ishak et al. [5] worked on the flow of the

stagnation point (SP) over a shrinking sheet using the MP fluid. Ameer et al. [6] used the microchannels to discuss the laminar behavior of the flow using a detailed theory of the MP fluid. Nazar et al. [7] also studied the SP flow of the MP fluid towards the stretching surface. The detail of the boundary layer flow using the MP fluid along with its results is demonstrated by Rees and Bassom [8]. Mitarai et al. [9] worked on the collisional granular flow, which is a type of the MP fluid. Galdi et al. [10, 11] proved that the equations based on the MP fluid can be solved and give unique solutions. A brief study published by the authors proved that the MP fluid equations have unique solutions. Mishra [12] worked on the peristaltic pumping of the MP fluid in a tube and presented numerical results. Particularly, the consequences of MP fluids have been displayed to the theory of lubrication and porous media, see Ref [13–19].

Beg et al. [18] did recent investigation about computation of nonisothermal and thermoconvective micropolar fluid dynamics in a Hall magnetohydrodynamic (MHD) generator system with nonlinear distending wall. Shamshuddin et al. [20] described discussion about micropolar fluid flow, which is induced due to a stretching sheet with heat source/sink and thermosolute chemically reacting micropolar fluid past a permeable stretching porous sheet. Beg et al. [21, 22] found facts about the experimental study of rheology and lubricity of drilling fluids enhanced with nanoparticles, and they published their findings about modeling magnetic nanopolymer flow with induction and nanoparticle solid volume fraction effects. Sheri and Shamshuddin [23] explored the facts about finite element analysis on transient MHD free convective chemically reacting micropolar fluid flow past a vertical porous plate with Hall current and viscous dissipation. Siva and Shamshuddin [24] investigated about transportation of heat in MHD flow along with chemical reaction and viscous dissipation. Shamshuddin et al. [25–27] worked on Lie symmetry analysis and numerical solutions for thermosolutal chemically reacting radiative micropolar flow, finite element computation of multiphysical micropolar transport phenomena from an inclined moving plate in the porous media, and Adomian decomposition method simulation of von Kármán swirling bioconvection nanofluid flow.

The Brownian motion (BM) is a motion of random particles and plays a vital role in the area of science and biology. The BM is produced due to the continuous bombardment of the molecules in the surrounding medium. This sort of motion is the result of the collision with nearby liquids/gaseous molecules. The mini/microscopic particles suspended in liquids or gases are impacted by the molecules of the fluid covering the particles. Sui et al. [28] studied the transportation of mass, collective motion, and BM. Mendoza-Gonzalez et al. [29] explained the continuous martingales and BM along with the continuity of nanoparticles and transformation of mass. Saffman and Delbruck [30] described the impacts of BM over chemical reactions in the thin sheet of a viscous fluid along with the chemical reactions. Michaelides [31] discussed the nanoparticle suspension during the movement of the liquid. Berla et al. [32]

discussed the role of BM, especially in the field of biology. The relation between BM and thermal conductivity is so strong, and by using this fact, Jang and Choi [33] proved that the main cause of BM is the increase in thermal conductivity. The effectiveness of BM can be seen in the references [34–36].

Thermophoresis is the change in position/migration of the large structure molecules to a macroscopic temperature gradient. The phenomenon is observed due to the exhibition of different responses of particles. McNab and Meissen [37] discussed the inspection of thermophoresis in liquids and showed the mixture behavior of nanoparticles. Talbot et al. [38] worked to show the reactions of the mixture of nanoparticles at the heated surface. Piazza and Parola [39] revealed the temperature gradient effects and uses of thermophoresis in colloidal suspensions. Willemsen et al. [40] explored the study of the molecular interaction in microscale thermophoresis. Wienken et al. [41] analyzed the protein binding in biological liquids using microscale thermophoresis. Jerabek-Willemsen et al. [42] presented the comprehensive study about the microscale thermophoresis. Iacopini and Piazza [43] implemented the thermophoresis in proteins. Seidel et al. [44] worked on the quantity of thermophoresis under some challenging conditions of bimolecular interfaces. Jellum et al. [45] discussed the nanoparticle mixture.

The activation energy (AE) is used to proceed exergonic reactions or energy required to initiate the reactions. For this, some or entire chemical linkages in the substrate are broken to form a novel product. The AE does not depend upon the process of exergonic reaction and proceeds in the forward direction/endergonic. The AE would be larger at a constant transition state and needs extra efficient energy to reach the up-hill level of the transition state. The higher the activation energy, the slower the rate of a chemical reaction. In some sort of specific cases at high AE, a reaction does not happen without any input/gain of energy. Sastry et al. [46] discussed distinct dynamical regimes in the energy landscape of a glass-forming liquid. Cohen and Turnbull [47] explored the transport of molecules in both gases as well as liquids. Goldstein [48] worked on the glass transition and viscous liquids using the potential energy. Dey and Bradt [49] discussed the chemical reactions with liquid and thermophoresis. Johari and Goldstein [50] worked on viscous liquids and glass transition. In the industry of chemical engineering, the AE has many uses in the field of geothermal reservoirs, oil emulsions, mechanics of water, and food processing [51–58].

In this work, the effects of MP fluids with BM and thermophoresis are discussed. Moreover, the effect of AE and thermal conductivity is also studied. The equations of motion, angular momentum, temperature, and concentration along with the boundary conditions are listed for the MP fluid. The rest of the paper is organized as follows: Section 2 describes the physical state of the problem. Section 3 presents the designed methodology based on the shooting scheme. Section 4 shows the detailed results and discussions. The conclusions are listed in the last section of the study.

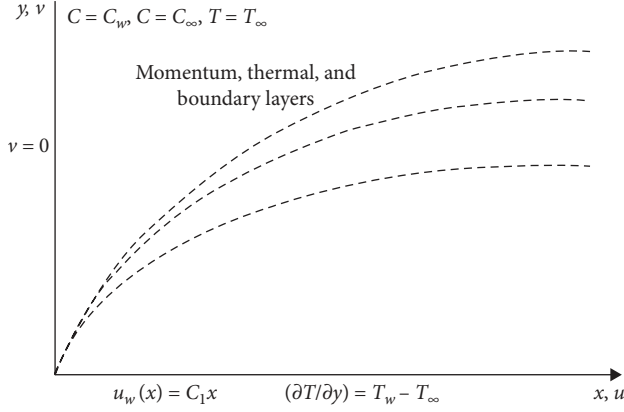


FIGURE 1: Analysis of the flow.

2. Physical Problem Statement

Consider a two-dimensional, incompressible, and steady flow involving mixed convection terms to the MP fluid over a semi-infinite stretching plate with the thermal diffusivity behavior of thermophoresis and BM. The convective surface and ambient temperature of the fluid are T_w and T_∞ , respectively, see Figure 1. The sheet surface and ambient concentrations are C_w and C_∞ , and the flow occupies within the domain $y > 0$. Stretchiness of the sheet occurs in the x -direction by holding the fixed origin, and the y -axis is perpendicular to it. The x -axis is taken towards the stretching plate, and the velocity of the sheet in the x -direction is $u = u_w(x) = c_1 x$. It is assumed that the chemical reaction is induced, and AE initiates the chemical reaction. The properties of the fluid are assumed to be constant in the steady case. Then, under the usual boundary layer approximations, the governing equations of continuity, linear momentum, angular momentum, equation of energy, and concentration are written as follows [59]:

$$\frac{\partial u}{\partial x} + \frac{\partial v}{\partial y} = 0, \quad (1)$$

$$u \frac{\partial u}{\partial x} + v \frac{\partial u}{\partial y} = \nu \frac{\partial^2 u}{\partial y^2} + K_1 \frac{\partial \sigma}{\partial y} + g_1 \beta^{**} (C - C_\infty) + g_1 \beta^* (T - T_\infty), \quad (2)$$

$$G_1 \frac{\partial^2 \sigma}{\partial y^2} - 2\sigma - \frac{\partial u}{\partial y} = 0, \quad (3)$$

$$u \frac{\partial T}{\partial x} + v \frac{\partial T}{\partial y} = \alpha \frac{\partial^2 T}{\partial y^2} + \tau \left\{ D_B \frac{\partial T}{\partial y} \frac{\partial C}{\partial y} + \frac{DT}{T_\infty} \left(\frac{\partial T}{\partial y} \right)^2 \right\}, \quad (4)$$

$$u \frac{\partial C}{\partial x} + v \frac{\partial C}{\partial y} = D_B \frac{\partial^2 C}{\partial y^2} + \frac{D_T (\rho c)_f}{(\rho c)_f T_\infty} \frac{\partial^2 T}{\partial y^2} - B_A (T_w - T_\infty)^w \exp \left\{ \frac{-E_a}{k(T - T_\infty)} \right\} (C - C_\infty). \quad (5)$$

The boundary conditions are

$$u = u_w(x) = c_1 x,$$

$$v = 0,$$

$$C = C_w,$$

$$\sigma = 0,$$

$$\frac{\partial T}{\partial y} = (T_w - T) \text{ at } y = 0,$$

$$\text{as } y \longrightarrow \infty, C \longrightarrow C_\infty, u \longrightarrow 0, T \longrightarrow T_\infty, \sigma \longrightarrow 0. \quad (6)$$

The following suitable transformations are introduced:

$$\Psi(x, y) = \sqrt{c_1 \nu} x f(\eta),$$

$$\theta(\eta) = \frac{T - T_\infty}{T_w - T_\infty}, \quad (7)$$

$$\phi(\eta) = \frac{C - C_\infty}{C_w - C_\infty},$$

$$\sigma = \sqrt{\frac{\alpha^3}{\nu}} x f(\eta),$$

$$u = \frac{\partial \Psi}{\partial y} = c_1 x f'(\eta),$$

$$v = -\frac{\partial \Psi}{\partial x} = -\sqrt{c_1 \nu} f(\eta), \quad (8)$$

$$\eta = y \sqrt{\frac{c_1}{\nu}},$$

where the stream function is Ψ . The transformations (7)–(8) are used in equations (1)–(5). Hence, we get the following system of ODEs:

$$f''' - f f'' + f'^2 + G_1 g' + G_r \theta + G_c \phi = 0, \quad (9)$$

$$G g'' - (2g + f'') = 0, \quad (10)$$

$$\theta'' + \text{Pr} \left(f \theta' + N b \theta' \phi' + N t \theta'^2 \right) = 0, \quad (11)$$

$$\phi'' + Sc f \theta' + \frac{Nt}{Nb} \theta'' - Sc \lambda^A \theta^w \exp\left(\frac{-E_a}{\theta}\right) \phi = 0. \quad (12)$$

The boundary conditions become

$$\begin{aligned} \theta'(0) &= Bi_\theta (1 - \theta(0)), \\ f(0) &= 0, \\ f'(0) &= 1, \\ g(0) &= 0, \\ \phi(0) &= 1, \\ \text{at } \eta &= 0, \\ f' &\longrightarrow 0, \\ g &\longrightarrow 0, \\ \theta &\longrightarrow 0, \\ \phi &\longrightarrow 0, \\ \text{as } \eta &\longrightarrow \infty. \end{aligned} \quad (13)$$

The parameters used in equations (9)–(12) are given as

$$\begin{aligned} G_1 &= \frac{K_1}{\nu}, \\ G_r &= \frac{gB^*(T_w - T_\infty)}{c_1 u_w}, \\ G_c &= \frac{gB^{**}(C_w - C_\infty)}{c_1 u_w}, \\ G &= \frac{G_1 \alpha}{\nu}, \\ Pr &= \frac{\nu}{\alpha}, \\ Nb &= \frac{\tau D_B (T_w - T_\infty)}{\nu}, \\ Nt &= \frac{D_T (C_w - C_\infty)}{\nu T_\infty}, \\ Sc &= \frac{\nu}{D_B}, \\ \lambda^A &= \frac{\nu B_A (T - T_\infty)^w}{c_1}, \\ Ea &= \frac{E_a}{T_w - T_\infty}, \\ Bi_\theta &= \sqrt{\frac{\gamma}{c_1}}. \end{aligned} \quad (14)$$

The shear stress and skin-friction coefficient is denoted and defined as:

$$\tau_w = \left| (\mu + S) \frac{du}{dy} + S\sigma \right|_{y=0}, \quad (15)$$

$$c_f = \left[\frac{2\tau_w}{\rho u^2} \right]_{y=0} = -2(Re_x)^{-0.5} f''(0),$$

where $Re_x = (c_1 x / \nu)$ is the local Reynolds number. From the temperature field, the rate of heat transfer is defined as

$$q_w = k \left[\frac{\partial T}{\partial y} \right]_{y=0}. \quad (16)$$

The coefficient of local heat transfer, local Nusselt number, and couple stress are given as

$$h(x) = \frac{q_w}{T_w - T_\infty}, \quad (17)$$

$$N_{ux} = \frac{h_x}{k} = (Re_x)^{-0.5} \theta'(0), \quad (18)$$

$$m_w = G_1 \left[\frac{\partial \sigma}{\partial y} \right]_{y=0} = (Re_x) \left(\frac{G_1 \alpha}{x} \right) g'(0). \quad (19)$$

Further, the local mass diffusion flux, local Sherwood number, takes the form as

$$Sh_x = \frac{x q_m}{D_B (C_w - C_\infty)}, \quad (20)$$

$$\frac{Sh_x}{(Re_x)^{0.5}} = -\phi(0), \quad (21)$$

where $q_m = -D_B [\partial C / \partial y]_{y=0}$.

The vector form of the skin-friction coefficient, the local Nusselt number, the couple stress number, and the Sherwood number, respectively, is given as

$$\begin{bmatrix} c_f (Re_x)^{0.5} \\ N_{ux} (Re_x)^{0.5} \\ \frac{m_w}{G_1 \alpha} x (Re_x)^{-0.5} \\ Sh_x (Re_x)^{-0.5} \end{bmatrix} = \begin{bmatrix} -2f''(0) \\ \theta'(0) \\ g'(0) \\ -\phi'(0) \end{bmatrix}. \quad (22)$$

3. Methodology

In order to present the solution of equations (9)–(12), the shooting scheme is applied [60–63]. The competency of this technique is to shoot the boundary conditions into initial conditions. Four initial conditions using $f(\eta)$, $g(\eta)$, $f'(\eta)$, $\theta(\eta)$, and $\phi(\eta)$ at $\eta \longrightarrow \infty$ were missing. The use of dummy conditions has been introduced instead of missing conditions. The numerical bvp4c obtained from the concepts

of the finite difference scheme is used to compare the numerical results.

Suppose

$$\begin{aligned} y_1' &= y_2, \\ y_2' &= y_3, \end{aligned} \quad (23)$$

$$\begin{aligned} y_3' &= y_1 y_3 - y_2^2 - G_1 y_9 - G_r y_4 - G_c y_6, \\ y_4' &= y_5, \\ y_5' &= \left[-Pr(y_1 y_5 - Nb y_7 y_5 - Nt y_5^2) \right], \end{aligned} \quad (24)$$

$$\begin{aligned} y_6' &= y_7, \\ y_7' &= \left[Sc \lambda^A (y_4)^w \exp\left(\frac{-E_a}{y_4}\right) y_6 - Sc y_1 y_5 + \frac{Nt}{Nb} y_5' \right], \end{aligned} \quad (25)$$

$$\begin{aligned} y_8' &= y_9, \\ y_9' &= \frac{1}{G} [2y_8 + y_3]. \end{aligned} \quad (26)$$

The concerned initial conditions are

$$\begin{aligned} y_1(0) &= y_2(0) = y_6(0) = y_8(0) = 1, \\ y_5(0) &= Bi_\theta (1 - y_4(0)) \text{ at } \eta = 0, \\ y_2(\eta) &\longrightarrow 0, \\ y_4(\eta) &\longrightarrow 0, \\ y_6(\eta) &\longrightarrow 0, \\ y_8(\eta) &\longrightarrow 0, \text{ as } \eta \longrightarrow \infty. \end{aligned} \quad (27)$$

4. Results and Discussion

The detailed results are provided in this section for solving the above system of equations using the shooting technique. The physical quantities related to various parameters are tabulated in Tables 1–3. Table 1 shows the explanation of the Nusselt and Sherwood numbers for the present study. Moreover, the discussions about behavior of local skin friction and couple stress of gas and water using different parameters are described in Tables 2 and 3, respectively. The result shows that by increasing Pr , the Nusselt number gradually increases and the Sherwood number decreases. To increase the BM coefficient, the local Nusselt number gives increasing effects, but the Sherwood number acts opposite to it. To increase the Schmidt number, the opposite behavior is noticed in the case of the Nusselt and Sherwood numbers. To increase the AE parameter, the local Nusselt number and Sherwood number results behave the same, but opposite results are noticed in the case of increasing the local Biot number.

The effects of coupling/interaction constant parameter G_1 , Grashof number G_r , concentration of thermal buoyancy ratio parameter G_c , microrotation parameter G , Nusselt number Nt , and AE parameter Ea on the local skin friction

TABLE 1: The variation of the Nusselt number and the Sherwood number with different parameters.

Pr	Nb	Sc	Ea	Bi _θ	θ'(0)	−ϕ'(0)
0.5	1	1	0.02	0.1	1.09871	−1.09571
1.0					1.09905	−1.09407
1.5					1.14013	−1.13016
	0.1				0.07876	−0.08620
	0.3				0.08908	−0.08895
	0.5				0.09017	−0.09682
		0.1			0.06216	−0.03907
		0.2			0.05404	−1.06539
		0.3			0.04313	−0.87672
				0.1	−0.08965	0.780897
				0.3	−0.09001	0.034500
				0.5	−0.09617	0.065432
			0.01		1.03271	−1.09527
			0.02		1.04504	−1.07574
			0.03		1.86018	−1.16048

TABLE 2: The behavior of local skin friction and couple stress number using different parameters for gases ($Pr < 1$).

G_r	G_c	G_1	Pr	G	Nt	Ea	−f''(0)	g'(0)
1.0	1.0	0.1	0.720	2.0	1	0.02	0.999213	0.2519962
1.5	—	—					1.408952	0.2928654
2.0	—	—					1.994673	0.3331887
	0.5	—					1.408955	0.2928693
	1.0						1.408959	0.2928665
	1.5						1.408956	0.2928653
		0.5					1.408953	0.2928657
		1.0					1.408955	0.2928657
		1.5					1.408950	0.2928645
			0.7				1.408951	0.2928656
			0.8				1.408956	0.2928654
			0.9				1.408953	0.2928652
				0.1			1.408958	0.2928651
				0.3			1.408954	0.2928667
				0.5			1.408957	0.2928655

and couple stress number for gases as well as for water are presented in Table 2 and 3.

For more investigations, several features based on physical dimensionless parameters are plotted in Figures 2–19 to investigate their physical impact on profiles of velocity, angular velocity, temperature, and concentration. Figure 2 shows the effects of the Grashof number G_r on the velocity. It is noticed that by increasing the values of G_r , the temperature gradient increases, and due to this fact, the velocity gradient increases. Figure 3 shows the thermal buoyancy ratio parameter G_c effects on the velocity profile. The velocity increases by increasing the values of G_c . Figure 4 depicts the coupling constant parameter G_1 effects on the velocity profile. As G_1 and coupling constant K_1 are directly related to each other and K_1 is in the flow theory, which determines the relative strength of interaction between particles or fields, so due to this increment in values of G_1 , the velocity profile decreases. Figure 5 represents the microrotation parameter G ; by increasing the values of G ,

TABLE 3: The behavior of local skin friction and couple stress number using different parameters for water ($P_r = 2$).

G_r	G_c	G_1	Pr	G	Nt	Ea	$-f''(0)$	$g'(0)$
1.0	1.0	0.1	2.0	2.0	1	0.02	0.999213	0.2519962
1.5	—	—					1.408952	0.2928654
2.0	—	—					1.994673	0.3331887
	0.5	—					1.408955	0.2928693
	1.0						1.408959	0.2928665
	1.5						1.408956	0.2928653
		0.5					1.408953	0.2928657
		1.0					1.408955	0.2928657
		1.5					1.408950	0.2928645
			2.0				1.408951	0.2928656
			2.5				1.408956	0.2928654
			3.0				1.408953	0.2928652
				0.1			1.408958	0.2928651
				0.3			1.408954	0.2928667
				0.5			1.408957	0.2928655

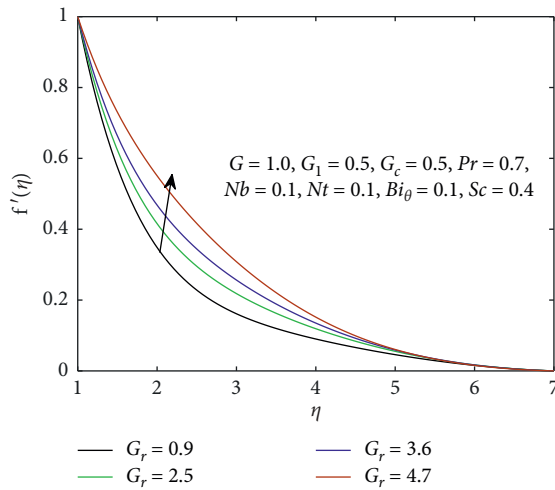


FIGURE 2: G_r effects on the velocity profile.

the velocity decreases due to rotation. When the rotation is involved, the linear motion goes down and angular velocity increases. Figure 6 shows that with the greater values of the microrotation parameter G , angular velocity increases because when the rotation increases, angular velocity also increases. Figures 7–11 indicate the effect of Pr , Sc , Nt , Nb , and Bi_θ on the temperature profile. The Schmidt number Sc is inversely related to the BM parameter. The increase in the values of Sc , increases the temperature profile. These results are indicated in Figure 7. Similarly, the Pr values and thermal conductivity are inversely related to each other. The reason is that when Pr increases, the thermal conductivity decreases, and due to this, the temperature profile decreases, as indicated in Figure 8. The observations of the thermophoresis parameter Nt are plotted in Figure 9, and the constant temperature profile decreases by increasing the values of Nt . By increasing the value of the BM parameter Nb , the random motion of the random particles interacts, and this interaction of these particles becomes the reason of the growing temperature. In Figure 10, the representation of the

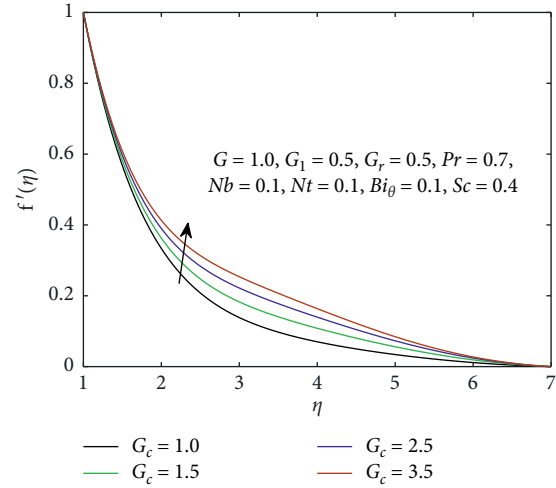


FIGURE 3: G_c effects on the velocity profile.

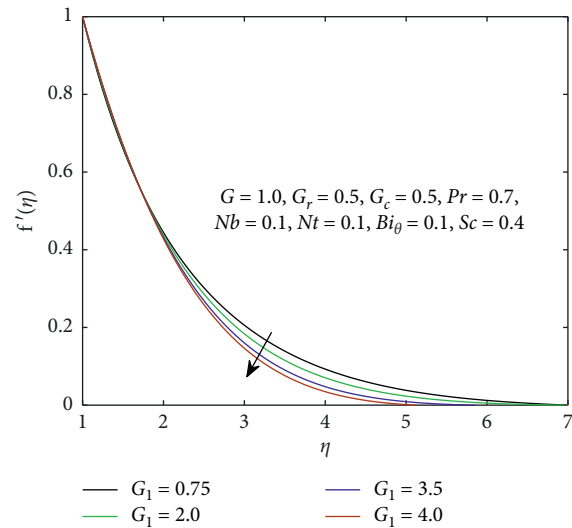
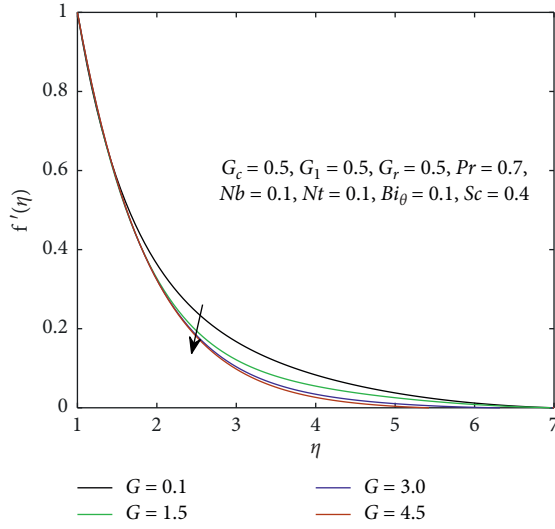
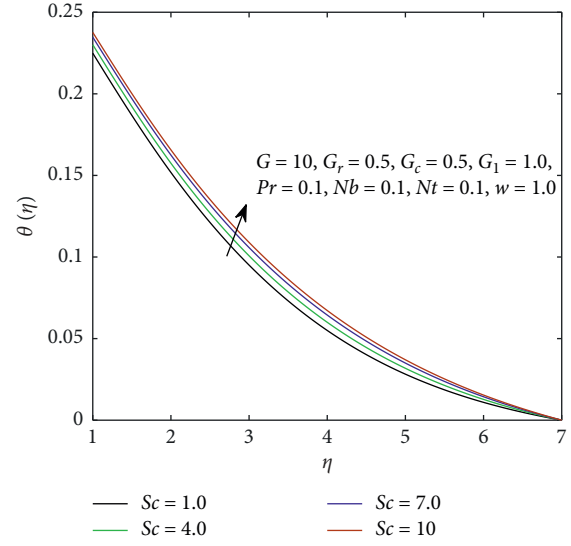
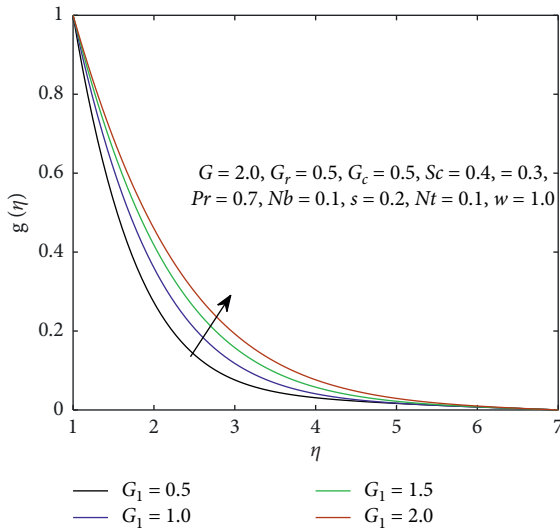
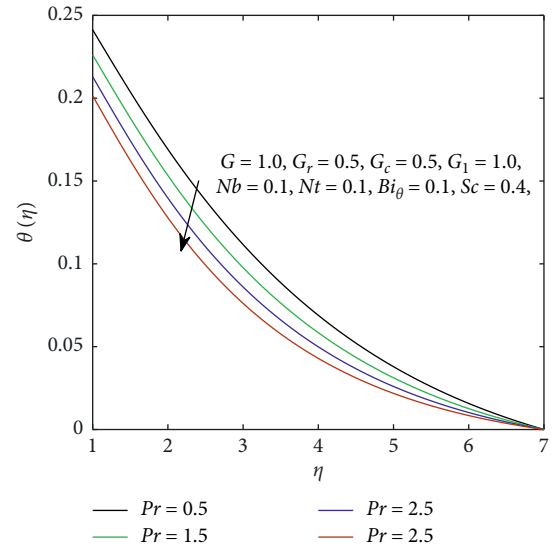


FIGURE 4: G_1 effects on the velocity profile.

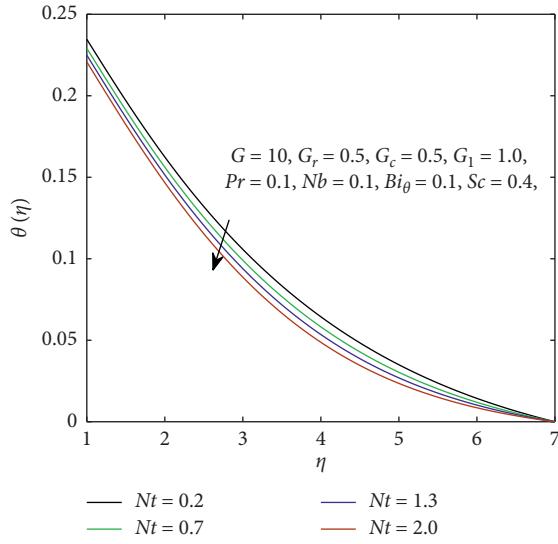
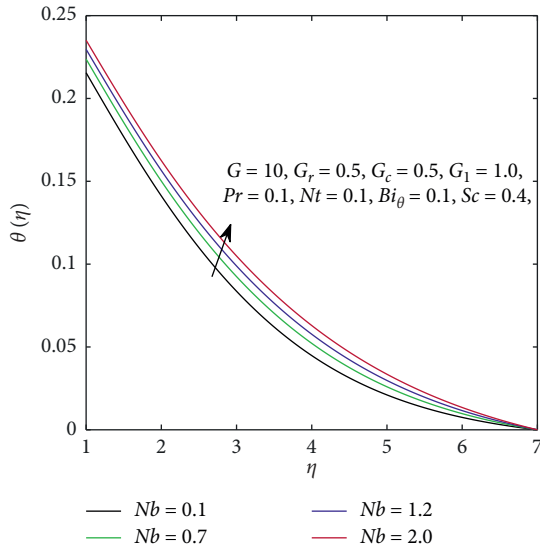
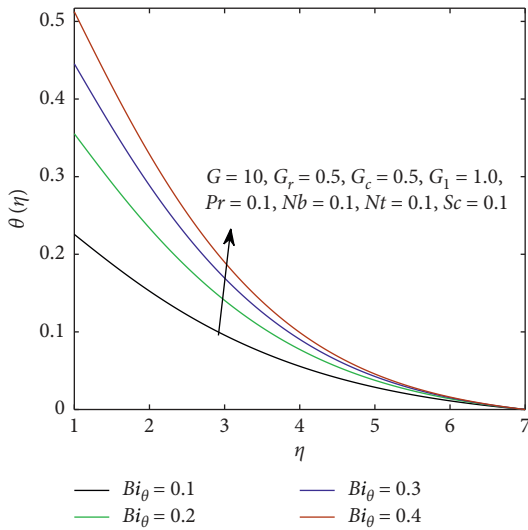
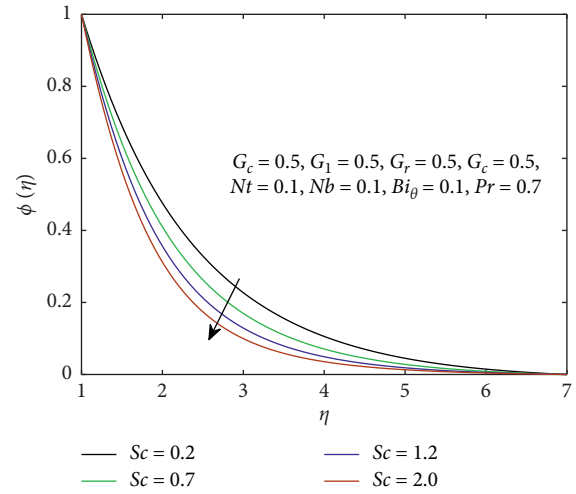
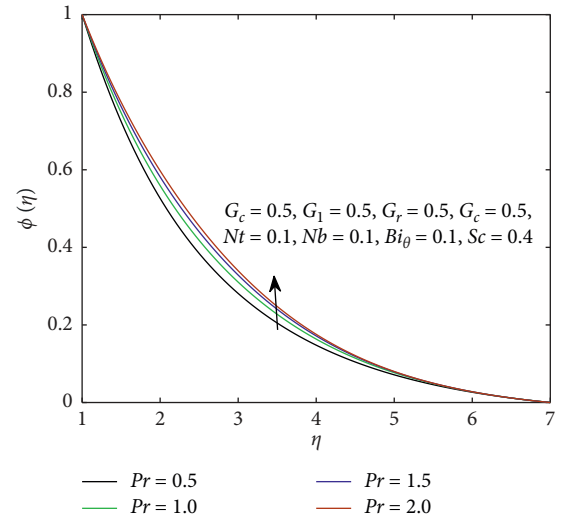
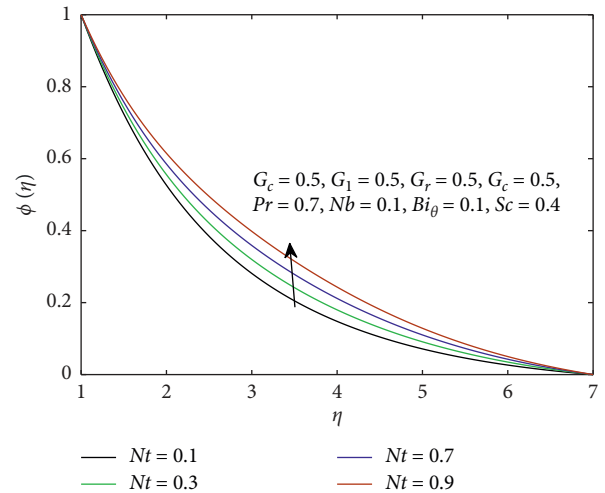
temperature variation using the values of Nb is presented. The thermal Biot number represents the thermal activity, and it increases by increasing the temperature profile which is also seen in Figure 11.

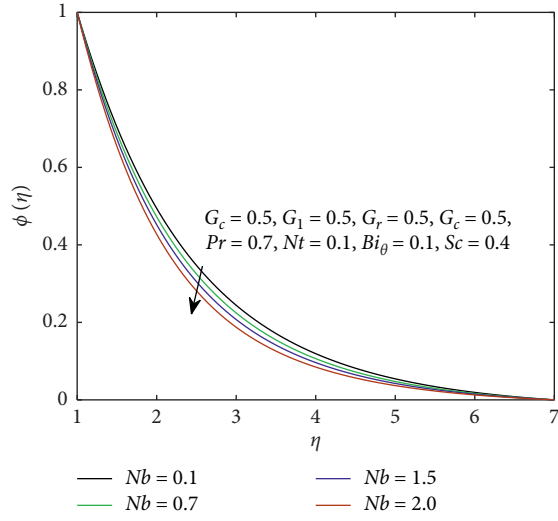
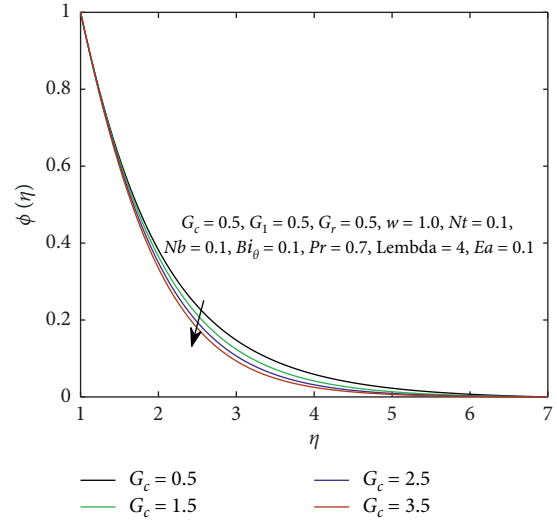
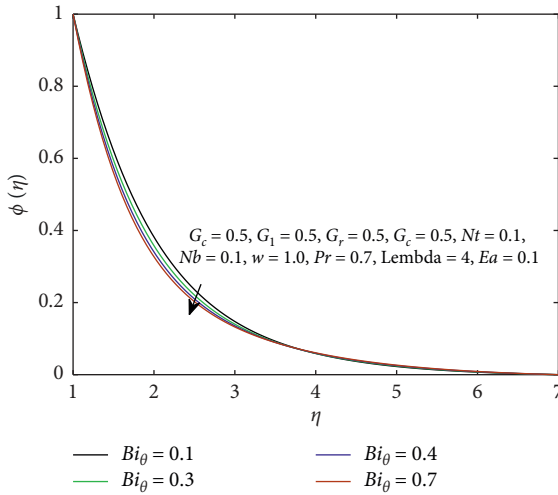
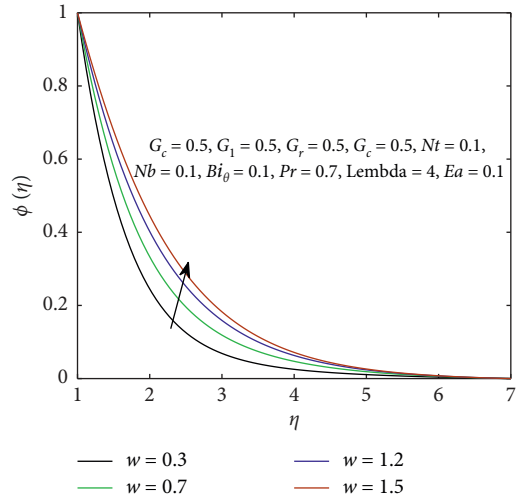
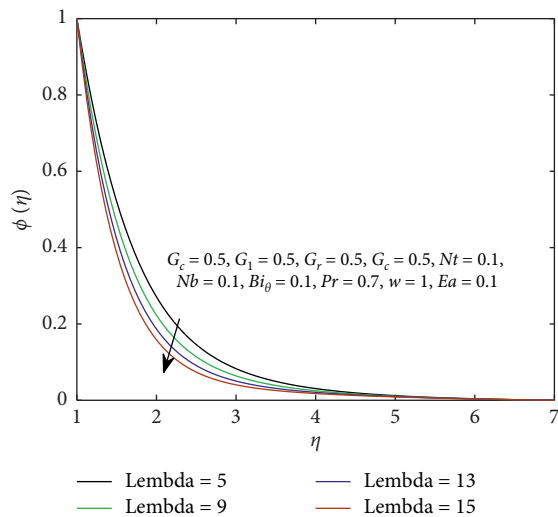
The effects of Sc , Pr , Nt , Nb , Bi_θ , G_c , and λ^A on the concentration profile are demonstrated in Figures 2–19. It is noticed that by increasing the values of Sc and Nb , the concentration profile decreases. Concentration field and its related boundary layer thickness decrease by uplifting the (Sc) Schmidt number. Actually, this Schmidt number is the ratio of viscosity to mass diffusivity. When the Schmidt number increases, then mass diffusivity decreases and results in reduction in the fluid concentration. Similarly, it is noticed that the nanoparticle concentration field diminishes, and its related concentration boundary layer thickness depreciates by increasing the values of Brownian motion. The Brownian motion takes place due to the presence of nanoparticles and resulted in the depreciation of nanoparticle concentration thickness.

FIGURE 5: G effects on the velocity profile.FIGURE 7: Sc effects on the temperature profile.FIGURE 6: G effects on angular momentum.FIGURE 8: Pr effects on the temperature profile.

Figures 12–15 represent that by increasing the values of Prand Nt , the concentration profile shows increasing behavior. By increasing Prandtl number, the velocity gradient increases, and due to this, the concentration also increases. Similarly, it is concluded that the concentration field enhances by increasing the values of the thermophoresis parameter (Nt) because concentration boundary layer thickness is an enhancing function of Nt .

The concentration profile decreases by increasing Bi_θ because thermal activity decreases with the mass transfer. Figures 16–19 indicate that with the increasing values of λ^A and G_c , the concentration profile decreases. Concentration increases for λ^A due to the Arrhenius function, and AE increases with the reduction of this function.

FIGURE 9: Nt effects on the temperature profile.FIGURE 10: Nb effects on the temperature profile.FIGURE 11: Bi_θ effects on the temperature profile.FIGURE 12: Sc effects on the concentration profile.FIGURE 13: Pr effects on the concentration profile.FIGURE 14: Nt effects on the concentration profile.

FIGURE 15: Nb effects on the concentration profile.FIGURE 18: G_c effects on the concentration profile.FIGURE 16: Bi_θ effects on the concentration profile.FIGURE 19: w effects on the concentration profile.FIGURE 17: λ^A effects on the concentration profile.

5. Conclusion

The present study is about to present the effects of activation energy and thermophoretic diffusion of nanoparticles on steady micropolar fluid along with Brownian motion. The designed model is solved using a famous shooting technique. Some root outcomes of the present study are as given in the following:

- (1) For a greater number of G_r , the profile of velocity increases. Increment in G_r means increment in the temperature gradient that causes an increase in the velocity distribution.
- (2) When there is an increase in the values of the coupling constant parameter G_1 , the velocity profile decreases.
- (3) The increasing values of the microrotation G show decrease in the velocity profile due to rotation, and the linear motion decreases and the angular velocity profile increases.

- (4) By increasing the value of Nt , the phenomenon of shifting the molecules from one place to another and the boundary layer thickness increase, which cause an increase in the concentration profile.
- (5) The temperature profile decreases with enhancing the parameter of thermophoresis Nt . By increasing the values of Nt , the thermal and concentration boundary layer thicknesses are increased, while increasing the BM parameter Nb , the profile of temperature increases.
- (6) By increasing the dimensionless AE parameter λ^A , the nanoparticle concentration profile increases due to the Arrhenius function and AE increases with the reduction of this function.

Abbreviation

K_1 :	Coupling constant
S :	Constant fluid characteristic
Ea :	Activation energy coefficient
K :	Thermal conductivity
τ :	Ratio parameter
C :	Concentration of the fluid
T :	Temperature of the fluid
D_B :	Brownian motion coefficient
D_T :	Thermophoresis coefficient
T_∞ :	Infinite temperature
T_w :	Temperature of the plate
G_1 :	Microrotation constant
ρ :	Fluid density
g_1 :	Magnitude of the gravity
α :	Thermal diffusivity
c_p :	Specific heat
w :	Constant
B_A :	Preexponential factor
G_r :	Grashof number
G_c :	Buoyancy ratio parameter
G :	Microrotation parameter
Pr :	Prandtl number
Nb :	Brownian motion parameter
Nt :	Thermophoresis parameter
Sc :	Schmidt number
λ^A :	Activation energy parameter
Bi_θ :	Thermal Biot number
β^* :	Thermal expansion coefficient
β^{**} :	Mass diffusion coefficient
ν :	Kinematic viscosity
c_f :	Skin-friction coefficient
Re_x :	Local Reynolds number
N_{ux} :	Nusselt number
m_w :	Couple stress
Sh_x :	Sherwood number
σ :	Microrotation component.

Data Availability

No data were used to support this study.

Conflicts of Interest

The authors declare that they have no conflicts of interest.

References

- [1] A. Eringen, "Theory of micropolar fluids," *Indiana University Mathematics Journal*, vol. 16, no. 1, pp. 1–18, 1966.
- [2] J. Peddieson, "An application of the micropolar fluid model to the calculation of a turbulent shear flow," *International Journal of Engineering Science*, vol. 10, no. 1, pp. 23–32, 1972.
- [3] P. G. Siddheshwar and S. Pranesh, "Magnetocovection in a micropolar fluid," *International Journal of Engineering Science*, vol. 36, no. 10, pp. 1173–1181, 1998.
- [4] A. C. Eringen, "Simple microfluids," *International Journal of Engineering Science*, vol. 2, no. 2, pp. 205–217, 1964.
- [5] A. Ishak, Y. Y. Lok, and I. Pop, "Stagnation-point flow over a shrinking sheet in a micropolar fluid," *Chemical Engineering Communications*, vol. 197, no. 11, pp. 1417–1427, 2010.
- [6] I. Papautsky, T. Ameel, and A. B. Frazier, "A review of laminar single-phase flow in microchannels," in *Proceedings of the ASME, Proceedings of International Mechanical Engineering Congress & Exposition Proc (IMECE)*, vol. 2, pp. 3067–3075, New York, NY, USA, November 2001.
- [7] R. Nazar, N. Amin, D. Filip, and I. Pop, "Stagnation point flow of a micropolar fluid towards a stretching sheet," *International Journal of Non-linear Mechanics*, vol. 39, no. 7, pp. 1227–1235, 2004.
- [8] D. A. S. Rees and A. P. Bassom, "The Blasius boundary-layer flow of a micropolar fluid," *International Journal of Engineering Science*, vol. 34, no. 1, pp. 113–124, 1996.
- [9] N. Mitarai, H. Hayakawa, and H. Nakanishi, "Collisional granular flow as a micropolar fluid," *Physical Review Letters*, vol. 88, no. 17, Article ID 174301, 2002.
- [10] G. P. Galdi and S. Rionero, "A note on the existence and uniqueness of solutions of the micropolar fluid equations," *International Journal of Engineering Science*, vol. 15, no. 2, pp. 105–108, 1977.
- [11] G. P. Galdi, A. Vaidya, M. Pokorný, D. D. Joseph, and J. Feng, "Orientation of symmetric bodies falling in a second-order liquid at nonzero Reynolds number," *Mathematical Models and Methods in Applied Sciences*, vol. 12, no. 11, pp. 1653–1690, 2002.
- [12] B. Mohanty, S. R. Mishra, and H. B. Pattanayak, "Numerical investigation on heat and mass transfer effect of micropolar fluid over a stretching sheet through porous media," *Alexandria Engineering Journal*, vol. 54, no. 2, pp. 223–232, 2015.
- [13] C. K. Selvi and A. N. S. Srinivas, "Oscillatory flow of a Casson fluid in an elastic tube with variable cross section," *Applied Mathematics and Nonlinear Sciences*, vol. 3, no. 2, pp. 571–582, 2018.
- [14] G. G. Krishna, S. Sreenadh, and A. N. S. Srinivas, "Entropy generation in couette flow through a deformable porous channel," *Applied Mathematics and Nonlinear Sciences*, vol. 4, no. 2, pp. 575–590, 2019.
- [15] R. Mourgues and P. R. Cobbold, "Some tectonic consequences of fluid overpressures and seepage forces as demonstrated by sandbox modelling," *Tectonophysics*, vol. 376, no. 1–2, pp. 75–97, 2003.
- [16] R. Ahmad, A. Farooqi, J. Zhang, and N. Ali, "Steady flow of a power law fluid through a tapered non-symmetric stenotic tube," *Applied Mathematics and Nonlinear Sciences*, vol. 4, no. 1, pp. 255–266, 2019.

- [17] M. P. Juniper and S. M. Candel, "The stability of ducted compound flows and consequences for the geometry of co-axial injectors," *Journal of Fluid Mechanics*, vol. 482, pp. 257–269, 2003.
- [18] O. A. Beg, M. Ferdows, M. E. Karim et al., "Computation of non-isothermal thermo-convective micropolar fluid dynamics in a Hall MHD generator system with non-linear distending wall," *International Journal of Applied and Computational Mathematics*, vol. 6, no. 2, pp. 1–44, 2020.
- [19] K. V. Prasad, H. Vaidya, and K. Vajravelu, "MHD mixed convection heat transfer over a non-linear slender elastic sheet with variable fluid properties," *Applied Mathematics and Nonlinear Sciences*, vol. 2, no. 2, pp. 351–366, 2017.
- [20] M. D. Shamshuddin, T. Thumma, and S. R. Mishra, "Thermosolutal chemically reacting micropolar fluid past a permeable stretching porous sheet," *Defect and Diffusion Forum*, vol. 392, pp. 42–59, 2019.
- [21] O. A. Bég, D. E. S. Espinoza, A. Kadir, M. Shamshuddin, and A. Sohail, "Experimental study of improved rheology and lubricity of drilling fluids enhanced with nano-particles," *Applied Nanoscience*, vol. 8, no. 5, pp. 1069–1090, 2018.
- [22] O. A. Bég, S. Kuharat, M. Ferdows, M. Das, A. Kadir, and M. Shamshuddin, "Modeling magnetic nanopolymer flow with induction and nanoparticle solid volume fraction effects: solar magnetic nanopolymer fabrication simulation," *Proceedings of the Institution of Mechanical Engineers, Part N: Journal of Nanomaterials, Nanoengineering and Nanosystems*, vol. 233, no. 1, pp. 27–45, 2019.
- [23] S. Sheri and M. D. Shamshuddin, "Finite element analysis on transient magnetohydrodynamic (MHD) free convective chemically reacting micropolar fluid flow past a vertical porous plate with Hall current and viscous dissipation," *Propulsion and Power Research*, vol. 7, no. 4, pp. 353–365, 2018.
- [24] R. S. Siva and M. D. Shamshuddin, "Heat and mass transfer on the MHD flow of micropolar fluid in the presence of viscous dissipation and chemical reaction," *Procedia Engineering*, vol. 127, pp. 885–892, 2015.
- [25] M. Shamshuddin, S. R. Mishra, O. A. Bég, and A. Kadir, "Lie symmetry analysis and numerical solutions for thermosolutal chemically reacting radiative micropolar flow from an inclined porous surface," *Heat Transfer-Asian Research*, vol. 47, no. 7, pp. 918–940, 2018.
- [26] M. Shamshuddin, O. Anwar Bég, M. Sunder Ram, and A. Kadir, "Finite element computation of multi-physical micropolar transport phenomena from an inclined moving plate in porous media," *Indian Journal of Physics*, vol. 92, no. 2, pp. 215–230, 2018.
- [27] M. D. Shamshuddin, S. R. Mishra, O. Anwar Beg, and A. Kadir, "Adomian decomposition method simulation of von Kármán swirling bioconvection nanofluid flow," *Journal of Central South University*, vol. 26, no. 10, pp. 2797–2813, 2019.
- [28] J. Sui, P. Zhao, Z. Cheng, and M. Doi, "Influence of particulate thermophoresis on convection heat and mass transfer in a slip flow of a viscoelasticity-based micropolar fluid," *International Journal of Heat and Mass Transfer*, vol. 119, pp. 40–51, 2018.
- [29] N. Y. Mendoza-Gonzalez, B. M. Goortani, and P. Proulx, "Numerical simulation of silica nanoparticles production in an RF plasma reactor: effect of quench," *Materials Science and Engineering: C*, vol. 27, no. 5–8, pp. 1265–1269, 2007.
- [30] P. G. Saffman and M. Delbruck, "Brownian motion in biological membranes," *Proceedings of the National Academy of Sciences*, vol. 72, no. 8, pp. 3111–3113, 1975.
- [31] E. E. Michaelides, "Brownian movement and thermophoresis of nanoparticles in liquids," *International Journal of Heat and Mass Transfer*, vol. 81, pp. 179–187, 2015.
- [32] B. M. Berla, R. Saha, C. M. Immethun, C. D. Maranas, T. S. Moon, and H. Pakrasi, "Synthetic biology of cyanobacteria: unique challenges and opportunities," *Frontiers in Microbiology*, vol. 4, p. 246, 2013.
- [33] S. P. Jang and S. U. S. Choi, "Role of Brownian motion in the enhanced thermal conductivity of nanofluids," *Applied Physics Letters*, vol. 84, no. 21, pp. 4316–4318, 2004.
- [34] D. Ernst, M. Hellmann, J. Köhler, and M. Weiss, "Fractional Brownian motion in crowded fluids," *Soft Matter*, vol. 8, no. 18, pp. 4886–4889, 2012.
- [35] S. Kheifets, A. Simha, K. Melin, T. Li, and M. G. Raizen, "Observation of Brownian motion in liquids at short times: instantaneous velocity and memory loss," *Science*, vol. 343, no. 6178, pp. 1493–1496, 2014.
- [36] X. Xu and A. Raman, "Comparative dynamics of magnetically, acoustically, and Brownian motion driven microcantilevers in liquids," *Journal of Applied Physics*, vol. 102, no. 3, Article ID 034303, 2007.
- [37] G. S. McNab and A. Meisen, "Thermophoresis in liquids," *Journal of Colloid and Interface Science*, vol. 44, no. 2, pp. 339–346, 1973.
- [38] L. Talbot, R. K. Cheng, R. W. Schefer, and D. R. Willis, "Thermophoresis of particles in a heated boundary layer," *Journal of Fluid Mechanics*, vol. 101, no. 4, pp. 737–758, 1980.
- [39] R. Piazza and A. Parola, "Thermophoresis in colloidal suspensions," *Journal of Physics: Condensed Matter*, vol. 20, no. 15, Article ID 153102, 2008.
- [40] M. Willemsen, C. J. Wienken, D. Braun, P. Baaske, and S. Duhr, "Molecular interaction studies using microscale thermophoresis," *Assay and Drug Development Technologies*, vol. 9, no. 4, pp. 342–353, 2011.
- [41] C. J. Wienken, P. Baaske, U. Rothbauer, D. Braun, and S. Duhr, "Protein-binding assays in biological liquids using microscale thermophoresis," *Nature Communications*, vol. 1, no. 1, 2010.
- [42] M. Jerabek-Willemsen, T. André, R. Wanner et al., "Micro-Scale thermophoresis: interaction analysis and beyond," *Journal of Molecular Structure*, vol. 1077, pp. 101–113, 2014.
- [43] S. Iacopini and R. Piazza, "Thermophoresis in protein solutions," *Europhysics Letters (EPL)*, vol. 63, no. 2, pp. 247–253, 2003.
- [44] S. A. I. Seidel, P. M. Dijkman, W. A. Lea et al., "Microscale thermophoresis quantifies biomolecular interactions under previously challenging conditions," *Methods*, vol. 59, no. 3, pp. 301–315, 2013.
- [45] G. M. Jellum, J. E. Daugherty, and D. B. Graves, "Particle thermophoresis in low pressure glow discharges," *Journal of Applied Physics*, vol. 69, no. 10, pp. 6923–6934, 1991.
- [46] S. Sastry, P. G. Debenedetti, and F. H. Stillinger, "Signatures of distinct dynamical regimes in the energy landscape of a glass-forming liquid," *Nature*, vol. 393, no. 6685, pp. 554–557, 1998.
- [47] M. H. Cohen and D. Turnbull, "Molecular transport in liquids and glasses," *The Journal of Chemical Physics*, vol. 31, no. 5, pp. 1164–1169, 1959.
- [48] M. Goldstein, "Viscous liquids and the glass transition: a potential energy barrier picture," *The Journal of Chemical Physics*, vol. 51, no. 9, pp. 3728–3739, 1969.
- [49] D. Dey and R. C. Bradt, "Grain growth of ZnO during Bi₂O₃ liquid-phase sintering," *Journal of the American Ceramic Society*, vol. 75, no. 9, pp. 2529–2534, 1992.

- [50] G. P. Johari and M. Goldstein, "Viscous liquids and the glass transition. II. Secondary relaxations in glasses of rigid molecules," *The Journal of Chemical Physics*, vol. 53, no. 6, pp. 2372–2388, 1970.
- [51] J. Wu, Z. Chen, and N. J. Dovichi, "Reaction rate, activation energy, and detection limit for the reaction of 5-furoylquinoline-3-carboxaldehyde with neurotransmitters in artificial cerebrospinal fluid," *Journal of Chromatography B: Biomedical Sciences and Applications*, vol. 741, no. 1, pp. 85–88, 2000.
- [52] R. Ellahi, A. Zeeshan, F. Hussain, and A. Asadollahi, "Peristaltic blood flow of couple stress fluid suspended with nanoparticles under the influence of chemical reaction and activation energy," *Symmetry*, vol. 11, no. 2, p. 276, 2019.
- [53] W. A. Khan, F. Sultan, M. Ali, M. Shahzad, M. Khan, and M. Irfan, "Consequences of activation energy and binary chemical reaction for 3D flow of Cross-nanofluid with radiative heat transfer," *Journal of the Brazilian Society of Mechanical Sciences and Engineering*, vol. 41, no. 1, p. 4, 2019.
- [54] F. G. Awad, S. Motsa, and M. Khumalo, "Heat and mass transfer in unsteady rotating fluid flow with binary chemical reaction and activation energy," *PLoS One*, vol. 9, no. 9, Article ID e107622, 2014.
- [55] K.-L. Hsiao, "To promote radiation electrical MHD activation energy thermal extrusion manufacturing system efficiency by using Carreau-nanofluid with parameters control method," *Energy*, vol. 130, pp. 486–499, 2017.
- [56] M. Mustafa, J. A. Khan, T. Hayat, and A. Alsaedi, "Buoyancy effects on the MHD nanofluid flow past a vertical surface with chemical reaction and activation energy," *International Journal of Heat and Mass Transfer*, vol. 108, pp. 1340–1346, 2017.
- [57] A. R. Bestman, "Natural convection boundary layer with suction and mass transfer in a porous medium," *International Journal of Energy Research*, vol. 14, no. 4, pp. 389–396, 1990.
- [58] O. D. Makinde, P. O. Olanrewaju, and W. M. Charles, "Unsteady convection with chemical reaction and radiative heat transfer past a flat porous plate moving through a binary mixture," *Afrika Matematika*, vol. 22, no. 1, pp. 65–78, 2011.
- [59] A. Raptis, "Flow of a micropolar fluid past a continuously moving plate by the presence of radiation," *International Journal of Heat and Mass Transfer*, vol. 41, no. 18, pp. 2865–2866, 1998.
- [60] M. Umar, Z. Sabir, A. Imran, A. H. Wahab, M. Shoaib, and M. A. Z. Raja, "Three-dimensional flow of casson nanofluid over a stretched sheet with chemical reactions, velocity slip, thermal radiation and Brownian motion," *Thermal Science*, vol. 24, no. 5, p. 339, 2020.
- [61] M. Umar, R. Akhtar, Z. Sabir et al., "Numerical treatment for the three-dimensional eyring-powell fluid flow over a stretching sheet with velocity slip and activation energy," *Advances in Mathematical Physics*, vol. 2019, pp. 1–12, 2019.
- [62] Z. Sabir, R. Akhtar, Z. Zhiyu et al., "A computational analysis of two-phase casson nanofluid passing a stretching sheet using chemical reactions and gyrotactic microorganisms," *Mathematical Problems in Engineering*, vol. 2019, pp. 1–12, 2019.
- [63] Z. Sabir, A. Imran, M. Umar, M. Zeb, M. Shoaib, and M. Raja, "A numerical approach for two-dimensional Sutterby fluid flow bounded at a stagnation point with an inclined magnetic field and thermal radiation impacts," *Thermal Science*, p. 186, 2020.